Research on Chemical Intermediates
https://doi.org/10.1007/s11164-019-03742-2

Two stimulus-responsive carbazole-substituted D–π–A pyrone compounds exhibiting mechanochromism and solvatochromism

Dongqi Liu[1,2] · Yuqi Cao[1,2] · Xilong Yan[1,2,3] · Bowei Wang[1,2,3]

Received: 9 October 2018 / Accepted: 12 January 2019

Abstract

Two D–A compounds were designed and synthesized from 2,6-dimethyl-4-pyrone and carbazole compounds. Both of them exhibited unique fluorescence properties in the aggregated state. Red shifts of the spectrum of 102 nm and 130 nm were observed for **BCSP** and **CSP** on changing the solvent from *n*-hexane to N,N-dimethylformamide (DMF), viz. solvatochromism. This phenomenon induced by the intramolecular charge transfer (ICT) effect was confirmed by density functional theory calculations. Interestingly, they both displayed excellent blue-shifted mechanochromic behavior, which was investigated by powder x-ray diffraction (PXRD) analysis. The results of this study provide a new avenue for the design of organic mechanochromic materials that exhibit a blue-shifting chromatic trend. Based on the unusual response of the solid fluorescence to external mechanical forces, we believe that these materials may be useful in various regards for potential applications.

Keywords Pyrone · Mechanofluorochromic · Solvatochromism · Blue-shifted

---

Dongqi Liu and Yuqi Cao have contributed equally to this work.

Electronic supplementary material The online version of this article (https://doi.org/10.1007/s11164-019-03742-2) contains supplementary material, which is available to authorized users.

✉ Xilong Yan
yan@tju.edu.cn

✉ Bowei Wang
bwwang@tju.edu.cn

[1] School of Chemical Engineering and Technology, Tianjin University, Tianjin, People's Republic of China

[2] Collaborative Innovation Center of Chemical Science and Engineering, Tianjin, People's Republic of China

[3] Tianjin Engineering Research Center of Functional Fine Chemicals, Tianjin, People's Republic of China

Introduction

Recently, the design and synthesis of smart organic fluorescence materials have aroused extensive interest. Among them, materials that exhibit the so-called mechanofluorochromic (MFC) effect have attracted considerable attention due to their specific color change induced by external forces (grinding or pressing). To date, various kinds of fluorescent sensors [1], optoelectronic materials [2], and viscosity probes [3] have been successively developed based on these outstanding characteristics. However, most traditional organic fluorophores often suffer from the aggregation-caused quenching (ACQ) effect. This deleterious effect can lead to decreased luminescence at high concentrations and seriously inhibits the applications of luminophores [4, 5]. Fortunately, in 2001, Tang and colleagues discovered a unique phenomenon in silole compounds. These molecules show strong emission in the aggregated state but weak fluorescence in dilute solution, which is termed aggregation-induced emission (AIE) [6]. To date, various kinds of mechanochromic materials with this AIE property have been reported, including tetraphenylethene (TPE) derivatives [7], triphenylamine derivatives [8, 9], phenothiazine derivatives [10, 11], etc. Nowadays, investigation of organic molecules with alternating donor (D) and acceptor (A) segments is considered to be a fruitful avenue for design of MFC materials, often leading to remarkable bathochromic MFC behavior [12–14]. Nevertheless, less attention has been focused on designing hypsochromic mechanofluorochromic materials. Enlarging the family of blue-shifted AIE-MFC materials and revealing the mechanism underlying their specific MFC behavior are still challenging.

Based on previous study, the 2,6-divinyl-4-pyrone unit has been reported to be a good building block for construction of bathochromic MFC molecules [15–17]. Previously, we varied the molecular electron donors to regulate the packing pattern, which was expected to aid development of hypsochromic MFC materials. In the work presented herein, two D–π–A-type 4-pyrone derivatives, namely 2,6-bis((*E*)-4-(9-butyl-9*H*-carbazol-3-yl)styryl)-4*H*-pyran-4-one (**BCSP**) and 2,6-bis((*E*)-4-(9*H*-carbazol-9-yl)styryl)-4*H*-pyran-4-one (**CSP**), were designed and synthesized [15–20]. Both target compounds displayed specific fluorescence properties in dichloromethane (DCM)–hexane mixtures and a remarkable solvatochromic effect in different solvents. Density functional theory (DFT) calculations were carried out to clarify this effect. To our surprise, a unique hypsochromic mechanochromic behavior in contrary to expectations was observed. Furthermore, powder wide-angle X-ray diffraction (PXRD) was used to investigate the relationship between the structure of each molecule and their unique MFC behavior.

Experimental

Materials and characterization

All materials and solvents were purchased and used without further purification. Both target compounds were synthesized as depicted in Scheme 1. ^{1}H and ^{13}C nuclear magnetic resonance (NMR) spectra were recorded using a Bruker Avance 400 MHz spectrometer with $CDCl_3$ as solvent. Ultraviolet–visible (UV–Vis) spectra were obtained on an Evolution 300 UV–Vis spectrophotometer. Liquid photoluminescence spectra were obtained using a Hitachi F-2500 spectrophotometer, while solid photoluminescence spectra and fluorescence quantum yields were recorded

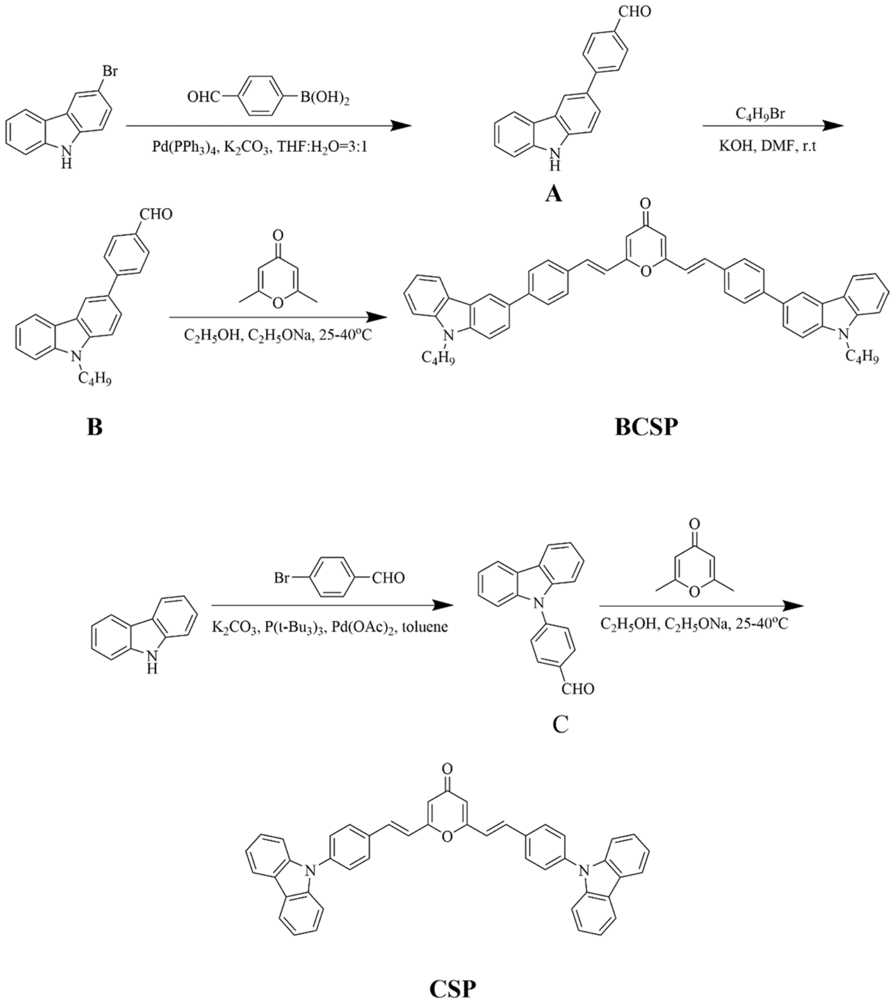

Scheme 1 Synthesis of **BCSP** and **CSP**

on a Horiba Jobin–Yvon Fluorolog-3 spectrophotometer. Dynamic light scattering (DLS) measurements were conducted on a Malvern Zetasizer Nano ZS90 size analyzer. XRD was performed on a Rigaka D/max 2500 X-ray diffractometer using Cu K_α radiation (40 kV, 40 mA) over the 2θ range from 5° to 60°. Density functional theory (DFT) calculations were performed using the Gaussian 09 package.

Synthesis of A

3-Bromocarbazole (10.00 g, 40.63 mmol), 4-(dihydroxyboryl)benzaldehyde (6.71 g, 44.72 mmol), K_2CO_3 (16.80 g, 121.82 mmol), and $Pd(PPh_3)_4$ (2.35 g, 2.04 mmol) were added in 80 mL tetrahydrofuran (THF)/water mixture (v/v = 3/1) under nitrogen atmosphere. After refluxing for 20 h, the mixture was cooled to room temperature, extracted with chloroform, and washed with brine. After drying over anhydrous sodium sulfate, the organic layer was evaporated. The resulting orange oil was purified by column chromatography using dichloromethane and petroleum ether as eluent to afford **A** as yellow solid (6.15 g, 55.81 %) [18].

Synthesis of B

A mixture of **A** (2.00 g, 7.37 mmol) and potassium hydroxide (2.07 g, 36.89 mmol) was dissolved in DMF (20.00 mL) and stirred for 0.5 h. 1-Bromobutane (2.02 g, 14.74 mmol) was slowly added to the above mixture. After stirring for 20 h at room temperature, the mixture was poured into water, and extracted with dichloromethane. The crude product was purified by column chromatography on silica gel using dichloromethane and petroleum ether as eluent to afford product **B** (2.22 g, 92.12 %) [19].

Synthesis of C

Carbazole (4.00 g, 23.92 mmol), 4-bromobenzaldehyde (5.00 g, 27.02 mmol), K_2CO_3 (8.30 g, 60.05 mmol), palladium acetate (0.40 g, 1.78 mmol), and tri-*tert*-butylphosphine (0.49 g, 2.42 mmol) were dispersed in 40 ml anhydrous toluene and refluxed for 24 h under nitrogen atmosphere. After the solvent had evaporated, the residue was purified by column chromatography to yield **C** as yellow solid (3.50 g, 53.85 %) [20].

Synthesis of BCSP and CSP

A mixture of 2,6-dimethyl-4-pyrone (0.25 g, 2.01 mmol) and **B** (5.00 mmol) was dissolved in ethyl alcohol (20.00 mL). Sodium ethoxide (0.34 g, 5.00 mmol) was added into the solution slowly. After stirring for 48 h at 40 °C, 5 % hydrochloric acid was used to adjust the pH to neutral. The crude product was extracted with dichloromethane, washed with brine, and dried over Na_2SO_4. After the solvent had evaporated, the mixture was purified by column chromatography (dichloromethane/ethyl acetate) and recrystallized in dichloromethane and ethyl acetate to afford the target compound **BCSP** (0.86 g, 57.5 %) [15, 16].

CSP was synthesized similarly to **BCSP**.

BCSP ^{1}H NMR (400 MHz, $CDCl_3$) δ 8.37 (s, 2H), 8.17 (d, $J=7.7$ Hz, 2H), 7.78 (dd, $J=14.2$, 8.4 Hz, 6H), 7.70 (d, $J=8.1$ Hz, 4H), 7.57 (d, $J=16.0$ Hz, 2H), 7.50 (t, $J=7.6$ Hz, 4H), 7.44 (d, $J=8.1$ Hz, 2H), 7.28 (d, $J=7.4$ Hz, 2H), 6.80 (d, $J=16.0$ Hz, 2H), 6.32 (s, 2H), 4.35 (t, $J=7.1$ Hz, 4H), 1.95–1.82 (m, 4H), 1.43 (dd, $J=15.1$, 7.5 Hz, 4H), 0.97 (t, $J=7.3$ Hz, 6H).^{13}C NMR (101 MHz, $CDCl_3$) δ 180.34, 161.43, 143.53, 140.99, 140.32, 135.71, 133.03, 131.00, 128.18, 127.55, 126.02, 124.92, 123.50, 122.95, 120.49, 119.21, 119.13, 118.79, 113.83, 109.13, 109.00, 43.00, 31.19, 20.61, 13.93. HRMS (ESI): calcd. for 743.3632 $(M+H)^+$, found 743.3630.

CSP ^{1}H NMR (400 MHz, $CDCl_3$) δ 8.15 (d, $J=7.7$ Hz, 4H), 7.81 (d, $J=8.0$ Hz, 4H), 7.65 (d, $J=8.1$ Hz, 4H), 7.58 (d, $J=16.0$ Hz, 2H), 7.49–7.40 (m, 8H), 7.31 (t, $J=7.2$ Hz, 4H), 6.84 (d, $J=16.0$ Hz, 2H), 6.37 (s, 2H). ^{13}C NMR (101 MHz, $CDCl_3$) δ 180.26, 161.17, 140.50, 139.07, 134.97, 133.84, 129.06, 127.28, 126.16, 123.71, 120.60, 120.49, 120.42, 114.44, 109.78. HRMS (ESI): calcd. for 653.2205 $(M+Na)^+$, found 653.2199.

Results and discussion

UV–Vis spectra

The absorption spectra of **BCSP** and **CSP** in dichloromethane are shown in Fig. S1. The peak at 300 nm for **BCSP** and at 292 nm for **CSP** can be attributed to π–π^* transitions. Meanwhile, both compounds presented another peak, located at 378 nm for **BCSP** and 342 nm for **CSP**, which can be ascribed to the intramolecular charge transfer (ICT) process in the D–A skeleton.

Photophysical properties of BCSP and CSP

To investigate the fluorescence properties of **BCSP** and **CSP** in the aggregated state, PL spectra were obtained in dichloromethane and *n*-hexane as a good and poor solvent, respectively. As shown in Fig. 1a, **BCSP** exhibited weak fluorescence in pure dichloromethane, which can be ascribed mainly to the random framework of the molecules in this good solvent and the nonradiative pathway accelerated by random molecular rotations. However, enhanced fluorescence of **BCSP** was observed on addition of *n*-hexane ($f_n < 70$ %) due to restriction of intramolecular rotation (RIR) (Fig. 1c) [21]. Upon addition of a poor solvent (*n*-hexane), the PL intensity reached a maximum at $f_n = 70$ %, with fluorescence quantum yield of 54.68 % for **BCSP** and 23.63 % for **CSP**. It is easy for these substituents to rotate freely around a single bond in dilute solution, which accelerates the nonradiative pathway. With

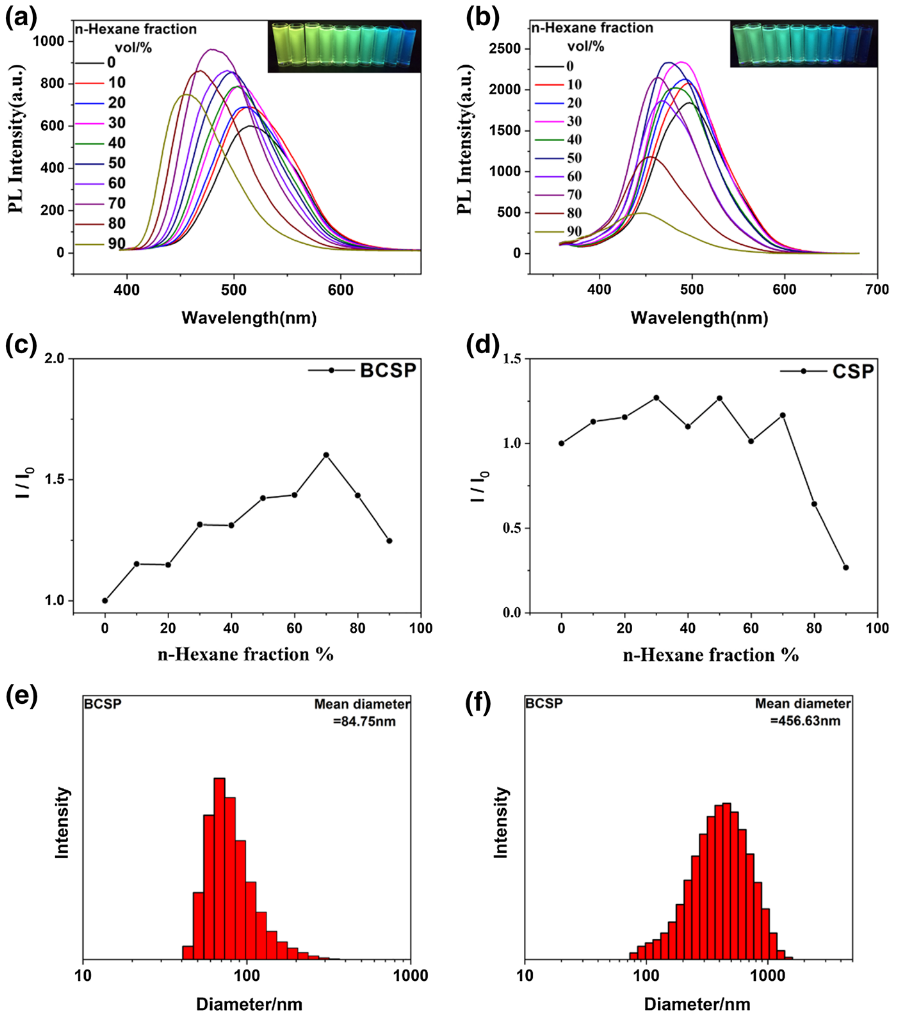

Fig. 1 PL spectra of compound **a BCSP** and **b CSP** in *n*-hexane/dichloromethane mixtures. Insets show emission images of the mixtures (365-nm UV lamp). **c**, **d** Relative emission intensity at different *n*-hexane fractions, where I_0 is the emission intensity in pure dichloromethane and I is the emission intensity at λ_{max}. **e**, **f** Particle size distribution of **BCSP** in DCM/*n*-hexane mixture at **e** 70 % (f_n) and **f** 90 % (f_n)

addition of *n*-hexane, such free rotation is impeded due to spatial constraints and the radiative relaxation pathway is further facilitated, resulting in aggregation of molecules and gradual enhancement of the emission [22]. Moreover, further addition of *n*-hexane induced formation of amorphous aggregates and decreased the emission intensity, especially for **CSP**. The size distribution of **BCSP** and **CSP** in the mixture was measured by DLS (Fig. 1e, f; Fig. S10). The average diameter of the nanoparticles presented an increase with increasing *n*-hexane fraction, further confirming the aggregation process and unique fluorescence behavior in the mixture [23]. Broadly speaking, the whole PL spectra displayed a hyperchromatic tendency, which can be ascribed to a decreased polarity upon addition of *n*-hexane.

The photophysical properties of **BCSP** and **CSP** were studied in solvents with different polarities. As illustrated in Fig. 2, red-shifts of the spectra of 102 nm and 130 nm were observed for **BCSP** and **CSP** on changing the solvent from *n*-hexane to DMF. This positive linear solvatochromic effect behavior on a Lippert–Mataga plot provides classical evidence for ICT. In addition, based on the linear response of the fluorescence to organic solvents, **BCSP** and **CSP** might be useful as colorimetric sensors [24]. In this regard, the charge separation condition in **BCSP** and **CSP** could be further stabilized by surrounding solvent molecules due to dipole–dipole interactions, reducing the energy gap between the highest occupied molecular orbital (HOMO) and lowest unoccupied molecular orbital (LUMO) levels [15, 16].

Density functional theory (DFT) calculations

DFT calculations on **BCSP** and **CSP** were carried out (Fig. 3) to further clarify the mentioned ICT effect. The electronic density in the HOMO level was mainly localized on electron-donating groups. In contrast, the LUMO level was distributed

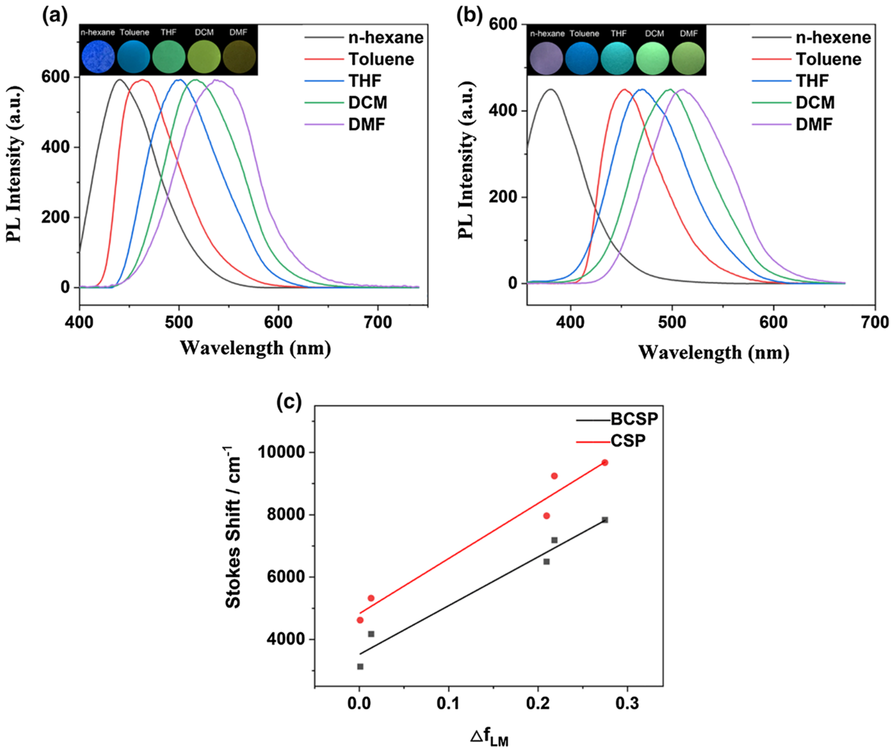

Fig. 2 Normalized PL spectra of **BCSP** (**a**) and **CSP** (**b**) in different solvents; **c** Lippert–Mataga plot of Stokes shift ($\Delta\nu$) of **BCSP** and **CSP** versus Δf in the solution

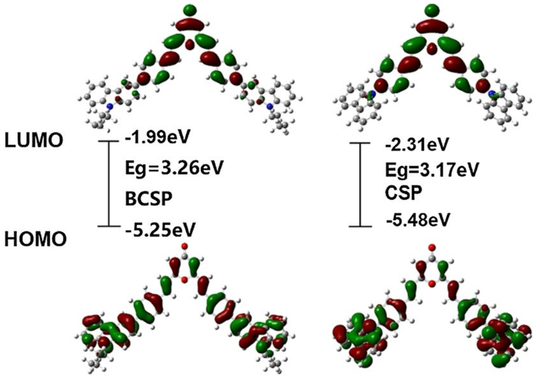

Fig. 3 Electron density distribution of HOMO and LUMO and energy gap for **BCSP** and **CSP**

mainly on the pyrone and phenyl rings. This prominent charge separation agrees well with the solvatochromic results described above and indicates the typical ICT effect [25].

Mechanochromic properties (MFC) and PXRD analysis of BCSP and CSP

The MFC behavior of **BCSP** and **CSP** is evaluated in Fig. 4. After grinding, the emission spectrum of the ground sample exhibited an unusual hypsochromic shift of 22 nm and 24 nm for **BCSP** and **CSP**, respectively. The fluorescence thus exhibited an obvious color change, accompanied by a remarkable change of the solid fluorescence quantum yield (Table 1; Fig. 4) [26]. Unfortunately, the fluorescence switching was irreversible. To gain insight into the molecular conformation of both compounds and their MFC behavior, their optimal molecular configuration was determined by DFT calculations (Figs. S2, S3). As illustrated in Fig. S2, one moderately planar conjugation skeleton was adopted in the molecule of **BCSP** with a dihedral angle between the bridge-linking phenyl rings and the substituted carbazolyl unit of 36°. It can therefore be deduced that **BCSP** might show a compact stacking

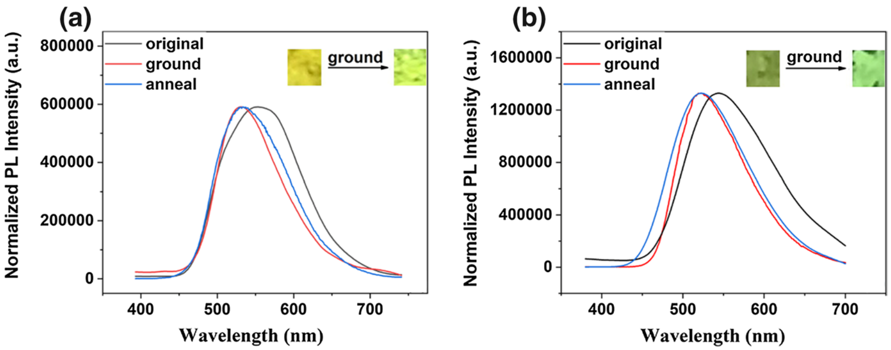

Fig. 4 Normalized PL emission spectra and fluorescence images of compounds in different solid states taken under a 365-nm UV lamp: **a BCSP**, **b CSP**

Table 1 Optical properties of **BCSP** and **CSP** in solution and solid state

Compound	Solution state			Solid state	
	λ_{abs} (nm)	ε (10^3 M^{-1} cm^{-1})		λ_{em} (nm)	ϕ_F (%)
BCSP	378	26.9	Original	552	18.54
			Ground	530	9.11
CSP	342	14.7	Original	542	13.01
			Ground	518	3.08

[a] Measured in dilute DCM solution

[b] ε measured at λ_{abs}

[c] Fluorescence quantum yield in solid state obtained using a calibrated integrating sphere

mode with strong intermolecular interactions in the original state due to its relatively planar molecular configuration [27]. In consequence, the mechanochromic mechanism of **BCSP** can be ascribed to destruction of such intermolecular interactions and a twisted conformation of the molecules [28, 29]. After grinding, a distorted molecular conformation might form, which would lead to the decrease of intermolecular interactions and π-conjugation. This is also demonstrated by the enhanced and blue-shifted emission after grinding. This interpretation also applies to **CSP**.

To confirm the change of the aggregation state in the original and ground form of the present compounds, powder X-ray diffraction (PXRD) experiments were performed. As shown in Fig. 5, the PXRD diffractograms of the pristine samples exhibited sharp scattering peaks, characteristic of a microcrystalline state. After grinding, the ground samples of **BCSP** displayed similarly reflections but with low intensity. The remaining crystalline features of the ground sample of **BCSP** can be attributed to an incomplete phase transition due to insufficient grinding force (Fig. 5a). Meanwhile, in the pattern for the ground **CSP** sample, most of the diffraction peaks were remarkably weakened or disappeared, indicating an amorphous state (Fig. 5b) [30,

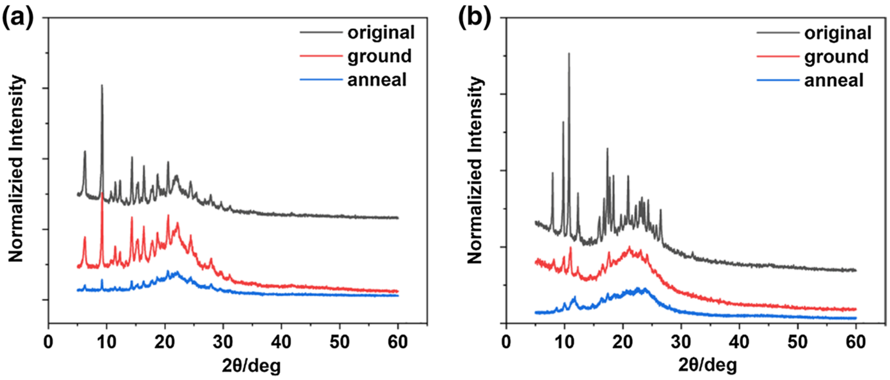

Fig. 5 Powder wide-angle X-ray diffraction (PXRD) patterns of compounds **a BCSP** and **b CSP** in different solid states

31]. Hence, the MFC behavior of **BCSP** and **CSP** can be related to the transformation from a crystalline to amorphous state. During this transformation, the intermolecular interactions are destroyed and the conformation of the molecules becomes more twisted, leading to the observed hypsochromic shift. Unfortunately, the diffraction signals of **BCSP** and **CSP** did not return to their original state after annealing treatment.

Conclusions

Two D–π–A-type 4-pyrone derivatives, viz. **BCSP** and **CSP**, were successfully synthesized and their photophysical properties investigated. The results showed that both of them exhibited obvious fluorescence properties in solution and a remarkable red-shifting solvatochromic effect. The specific ICT effect was confirmed by DFT calculations. More importantly, **BCSP** and **CSP** also displayed obvious blue-shifting MFC properties. The relationship between the MFC character and the molecular packing mode was revealed by PXRD analysis, and the mechanism can be ascribed to the transformation between a crystalline and amorphous state. This study promotes a strategy to design blue-shifting MFC materials by structural modulation. Based on the unusual response of the solid fluorescence to external mechanical forces, such materials might have potential applications in various directions [32].

References

1. P. Alam, V. Kachwal, I.R. Laskar, Sens. Actuators B **228**, 539 (2016)
2. J. Sim, H. Lee, K. Song, S. Biswas, A. Sharma, G.D. Sharma, J. Ko, J. Mater. Chem. C **4**, 3508 (2016)
3. H. Soleimaninejad, M.Z. Chen, X. Lou, T.A. Smith, Y. Hong, Chem. Commun. **53**, 2874 (2017)
4. D. Ding, K. Li, B. Liu, B.Z. Tang, Acc. Chem. Res. **46**, 2441 (2013)
5. B. Guo, X. Cai, S. Xu, S.M.A. Fateminia, J. Liu, J. Liang, G. Feng, W. Wua, B. Liu, J. Mater. Chem. B **4**, 4690 (2016)
6. B.Z. Tang, X. Zhan, G. Yu, P.P.S. Lee, Y. Liu, D. Zhu, J. Mater. Chem. **11**, 2974 (2001)
7. Y. Wang, D. Xu, H. Gao, Y. Wang, X. Liu, A. Han, C. Zhang, L. Zang, Dyes Pigments **156**, 291 (2018)
8. P. Xue, P. Chen, J. Jia, Q. Xu, J. Sun, B. Yao, Z. Zhang, R. Lu, Chem. Commun. **50**, 2569 (2014)
9. W.Z. Yuan, Y. Tan, Y. Gong, P. Lu, J.W.Y. Lam, X.Y. Shen, C. Feng, H.H.-Y. Sung, Y. Lu, I.D. Williams, J.Z. Sun, Y. Zhang, B.Z. Tang, Adv. Mater. **25**, 2837 (2013)
10. B. Xu, Y. Mu, Z. Mao, Z. Xie, H. Wu, Y. Zhang, C. Jin, Z. Chi, S. Liu, J. Xu, Y.-C. Wu, P.-Y. Lu, A. Lien, M.R. Bryce, Chem. Sci. **7**, 2201 (2016)
11. C. Arivazhagan, A. Maity, K. Bakthavachalam, A. Jana, S.K. Panigrahi, E. Suresh, A. Das, S. Ghosh, Chem. Eur. J. **23**, 1 (2017)
12. G. Yin, Y. Ma, Y. Xiong, X. Cao, Y. Li, L. Chen, J. Mater. Chem. C **4**, 751 (2016)
13. Y. Wang, D. Xu, H. Gao, Y. Wang, X. Liu, A. Han, C. Zhang, L. Zang, J. Phys. Chem. C **122**, 2297 (2018)
14. Z. Chi, X. Zhang, B. Xu, X. Zhou, C. Ma, Y. Zhang, S. Liu, J. Xu, Chem. Soc. Rev. **41**, 3878 (2012)
15. Y. Cao, L. Chen, Y. Xi, Y. Li, X. Yan, Mater. Lett. **212**, 225 (2018)
16. Y. Cao, Y. Xi, X.Y. Teng, Y. Li, X. Yan, L. Chen, Dyes Pigments **137**, 75 (2017)
17. Y. Cao, L. Chen, D. Liu, B. Wang, Sci. China Mater. (2018). https://doi.org/10.1007/s40843-018-9371-y
18. D. Karthik, K.R.J. Thomas, J.-H. Jou, Y.-L. Chen, Dyes Pigments **133**, 132 (2016)

19. Z. Li, Z. Li, C. Di, Z. Zhu, Q. Li, Q. Zeng, K. Zhang, Y. Liu, C. Ye, Z.J. Qin, Macromolecules **39**, 6951 (2006)
20. P. Xue, J. Sun, P. Chen, P. Wang, B. Yao, P. Gong, Z. Zhang, R. Lu, Chem. Commun. **51**, 10381 (2015)
21. L. Chen, Y. Jiang, H. Nie, R. Hu, H.S. Kwok, F. Huang, A. Qin, Z. Zhao, B.Z. Tang, ACS Appl. Mater. Interfaces **6**, 17215 (2014)
22. E. Horak, M. Robić, A. Šimanović, V. Mandić, R. Vianello, M. Hranjec, I.M. Steinberg, Dyes Pigments **162**, 688 (2019)
23. X. Zhang, X. Huang, X. Gan, Z. Wu, J. Yu, H. Zhou, Y. Tian, J. Wu, Sens. Actuators B **243**, 421 (2017)
24. H. Zhu, J. Huang, L. Kong, Y. Tian, J. Yang, Dyes Pigments **151**, 140 (2018)
25. R. Hu, E. Lager, A.A. Aguilar, J. Liu, J.W.Y. Lam, H.H.Y. Sung, I.D. Williams, Y. Zhong, K.S. Wong, E.P. Cabrera, B.Z. Tang, J. Phys. Chem. C **113**, 15845 (2009)
26. A. Kundu, S. Karthikeyan, D. Moon, S.P. Anthony, ChemistrySelect **3**, 7340 (2018)
27. Y. Zhan, P. Gong, P. Yang, Z. Jin, Y. Bao, Y. Lia, Y. Xu, RSC Adv. **6**, 32697 (2016)
28. J. Wu, Y. Cheng, J. Lan, D. Wu, S. Qian, L. Yan, Z. He, X. Li, K. Wang, B. Zou, J. You, J. Am. Chem. Soc. **138**, 12803 (2016)
29. J. Hu, J. Wang, R. Liu, Y. Li, J. Lu, H. Zhu, Dyes Pigments **153**, 84 (2018)
30. C. Ma, X. Zhang, L. Yang, Y. Li, H. Liu, Y. Yang, G. Xie, Y.-C. Ou, Y. Wei, Dyes Pigments **136**, 85 (2017)
31. P.S. Hariharan, D. Moon, S.P. Anthony, CrystEngComm **19**, 6489 (2017)
32. L. Zang, H. Shang, D. Wei, S. Jiang, Sens. Actuators B **185**, 389 (2013)